Anisotropic technical properties of building stones and their development due to fabric changes

DANIEL STROHMEYER & SIEGFRIED SIEGESMUND
Geowissenschaftliches Zentrum Goettingen, Strukturgeologie & Geodynamik, Goldschmidtstrasse 3, 37077 Goettingen, Germany (e-mail: dstrohm@gwdg.de)

Abstract: Technical properties of building stones are of critical importance in applied geosciences such as engineering geology, and also with respect to construction or building physics. Among the many factors which control the technical properties, special importance is given to the rock fabrics influencing the anisotropy of these technical properties. To demonstrate this relationship a sequence of mylonitic rocks, i.e. metagranitoid progressively deformed to mylonite and ultramylonite, was selected. The mineralogical and chemical composition of the protolith and mylonite is nearly identical. All investigated parameters (tensile strength, compressive strength, abrasive strength, magnetic susceptibility and ultrasound wave velocities) are anisotropic and finally controlled by the mineralogical composition and the different fabric elements like microstructural features, the crystallographic and shape preferred orientations and the state of microcracking. The development of the rock fabric with mylonitization, in particular the preferred orientation of mica, seems to be most important for the directional dependence of rock physical properties, at least in mica-rich rocks. However, various sets of microcracks, the degree of grain size reduction, the intensity of the foliation and the compositional layering can significantly modify the results. The interaction of superimposing parameters for different technical properties does not allow any simple cross-correlation.

The properties of dimensional stones, i.e. polycrystalline aggregates, are influenced by the properties and volume fraction of the rock-forming minerals. The selection of building stones is usually done for aesthetic reasons; however, their technical properties are not taken into consideration, which must satisfy certain requirements based on building physics. The reference standards of each country or at the European scale dictate the necessary requirements. For example, the suitability of dimensional stones for ventilated facades requires measurement of the flexural strength and freeze–thaw tests. In the case of marble panels (see discussion in Koch & Siegesmund 2002) the spectacular phenomenon of bowing is not considered by current European standard (EN) testing. Bowing has also been reported from gravestones made from granite (Winkler 1994).

Without any doubt the tests most often used are those that quantify the mechanical quality of dimensional stones. In most stone certifications a value of the Young's modulus or of the strength is given without any further qualification. This is highly questionable, since commonly, most of the rocks are anisotropic when considering physical properties (Siegesmund 1996). The assumption of isotropy is only valid for rocks with a random distribution of minerals, microcracks, pores etc. An anisotropic fabric can be caused by the crystallographic preferred orientation (here referred to as texture) of rock-forming minerals together with their shape-controlled anisotropy and the preferred orientation of microcracks. In consequence, an anisotropic rock fabric can produce a pronounced dependence of technical and physical properties. This is very important, since building stones may often be cut in different directions to enhance decorative effects. Furthermore, such directions do not coincide with the determined highest strength values. The importance of direction-dependent strength values is valid, for example, for overhead floors, brackets, architraves, balconies and staircases.

To demonstrate the effect of anisotropic rock fabrics on the physical properties we selected a sequence of mylonitic rocks, i.e. a metagranitoid that was transformed by ductile deformation to an ultramylonite (three samples: Iv1, Iv1b, Iv2). A progressive mylonitization is usually characterized by a process of grain size reduction compared to the protolith resulting from crystal plastic processes. These processes produce another characteristic feature of a deformed rock, a crystallographic preferred orientation.

From: SIEGESMUND, S., WEISS, T. & VOLLBRECHT, A. 2002. *Natural Stone, Weathering Phenomena, Conservation Strategies and Case Studies*. Geological Society, London, Special Publications, **205**, 115–135.
0305-8719/02/$15.00 © The Geological Society of London 2002.

In these rocks different physical properties like compressive strength, tensile strength, elastic wave velocities, the magnetic susceptibility and the abrasion strength were measured. The anisotropic physical properties are discussed in terms of the rock fabrics and the mineralogical composition.

Experimental

Mineralogical and fabric investigations

The mineralogical composition was determined by electron microprobe (Jeol JXA 8900) element mapping and phase analysis of three mutually perpendicular thin sections. Pore radii distributions were measured by mercury porosimetry. The texture of muscovite was determined by universal stage measurements in three mutually perpendicular thin sections. The microcrack distribution was assessed qualitatively with the universal stage. Neutron diffraction measurements (Leiss & Ullemeyer 1999) were performed in Dubna, Russia, on cylindrical samples with a diameter and a length of 40 mm to examine the texture of quartz and albite. Additional information concerning the texture of phyllosilicates was done by measuring the anisotropy of the magnetic susceptibility (AMS) using a KLY-2 Kappabridge and computed using the ANISO 11 program developed by Jelinek (1977).

Rock mechanical tests

All mechanical testing was performed in three mutually perpendicular directions by using a class I universal testing machine manufactured by Walter & Bay (Switzerland). For the tensile/compression and abrasive test (Boehme method) the samples were cored parallel to the x-, y-, z-axis of the reference system (Fig. 1) and sawn perpendicular to the x-, y-, z-axis of the reference system (Boehme method), respectively. The tensile strength was determined indirectly by using the Brazilian test following the recommendations of DIN 22024; however, the loading rate was 30 N s^{-1}. The sample sizes were 40 mm in diameter with a length of 20 mm. To determine the compressive strength the uniaxial compression test (UCS) after DIN EN 1926 was used. The samples were 50 mm in diameter and length. The increase in load was 1000 N s^{-1}. The abrasive strength was assessed by using the Boehme test as described in DIN 52108. References are also given in DIN EN 1341/1342/1343. To minimize the experimental error, five to 18 specimens (Brazilian and UCS) and two to three specimens (Boehme method) were measured in each direction, respectively.

Ultrasonic wave velocities

To estimate the three-dimensional distribution of open microcracks compressional wave velocities (*Vp*) of water-saturated and dry spheres (50 mm in diameter) were measured in 192 directions. All data were plotted in pole figures using the Schmidt net lower hemisphere (Fig. 1). To display the crack-induced rock anisotropy difference diagrams were calculated (*Vp* water-saturated minus *Vp* dry). The resonant frequency of the transmitter was 1 MHz. The spatial dependence of P-wave velocities studied

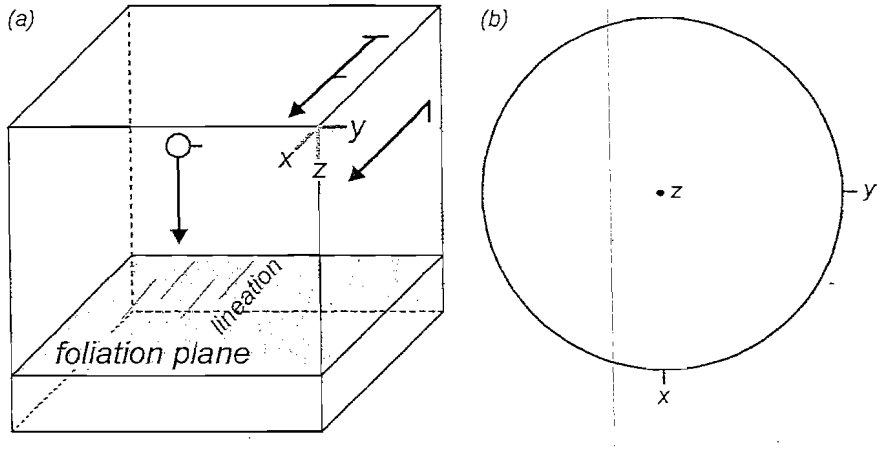

Fig. 1. (**a**) Marking system/reference system (arrows) used for delineation of the macroscopic visible foliation and lineation. (**b**) Depiction of pole figures and *Vp* pattern diagrams; Schmidt-net lower hemisphere; projection plane equal to foliation plane; z-axis vertical in the middle of the diagram.

on spherical samples allows the determination of velocities in a general triclinic body. If the spheres are investigated under dry and water-saturated conditions, material behaviour is highly influenced by pore fluid which can be used to diagnose the microcrack fabrics. The difference between the water-saturated and dry (air-filled) conditions is a powerful tool to quantify the open cracks via the *Vp* data. The effect of open cracks is reduced but not completely suppressed, because *Vp* compressibility of air is higher than that of water. The calculated ΔVp ($Vp_{saturated} - Vp_{dry}$) gives an idea about the crack-induced anisotropy (Schild *et al.* 2001). This method is comparable to the measurement of dry samples under various confining pressures as performed by Meglis *et al.* (1996), Duerrast *et al.* (1999) and Rasolofosoan *et al.* (2000). The *Vp* pattern of the water-saturated sample mainly shows the intrinsic anisotropy characterized by the preferred orientation of the rock-forming minerals, their single crystal anisotropy and their volume content (Siegesmund *et al.* 1993; Siegesmund 1996) and is dominated by highly anisotropic phyllosilicates. The trapped pore space cannot be water-saturated and contributes to the *Vp* anisotropy of the water-saturated specimen. Another factor is healed cracks which may form zones of anisotropy, but they do not affect the ultrasonic wave velocities. Hence, they may change due to an increasing degree of mylonitization without causing any changes concerning the ΔVp pattern.

In addition, ultrasonic wave velocity measurements were performed on cylindrical samples cored in three mutually perpendicular directions. Various confining pressures were applied from 2 to 400 MPa. The dimension of the samples was 30 mm in diameter and 35 mm in length. The running time of two mutually perpendicular shear waves and one compressional wave (resonant frequency 1 MHz) was simultaneously determined.

Rock samples and their fabrics

To investigate the fabric development of mylonites and its control on the mechanical and physical properties, a shear zone from the Sesia-Lanzo Zone (Italy) was chosen. Three samples were collected that are characterized by different degrees of mylonitization. The material was taken from the boundary and towards the centre of the shear zone. All samples show the same state of weathering. The more or less undeformed protolith (Iv1) is a metagranitoid overprinted under retrograde greenschist facies conditions. Iv1b and Iv2 are a mylonite and an ultramylonite, respectively. The mineralogical and chemical composition of all samples is nearly identical. Main constituents are plagioclase (albite), quartz and muscovite; garnet, K-feldspar, chlorite, clinozoisite/epidote are associated minerals and apatite and zircon occur as asseccories (Table 1). Macroscopically green coloured microcrystalline aggegates consist of chlorite, albite, garnet and sericite. Techmer (1996) considered these to be alterations originating from K-feldspar grains. The slight changes in the mineralogical composition within the shear zone are due to fluid–rock interactions. They are characterized by newly formed clinozoisite/epidote, muscovite and chlorite (Techmer 1996), while the clinozoisite/epidote content slightly increases towards the shear zone centre. Therefore, the subsidary changes in mineralogical composition should have no significant influence on the mechanical and physical rock properties.

The protolith (Iv1) exhibits an L-fabric. The elongated quartz crystals as well as the microcrystalline polyphase aggregates define a distinct lineation while a weakly developed macroscopic foliation can be deduced from slightly flattened quartz crystals. The mylonite (Iv1b) and the ultramylonite (Iv2) show all signs of an LS-fabric. The progressive and more narrow spaced foliation with increasing mylonitization is defined by the preferred orientation of minerals and grain boundaries as well as a distinct layering of quartz-, albite- and chlorite-clinozoisite/epidote-rich layers (Fig. 2).

The fabric development is accompanied by a distinct reduction in grain size. In Iv1 quartz as well as K-feldspar appears as large crystals with an average grain size of 1 to 3 mm. Recrystallized grains, subgrains and migrated grain boundaries are typical deformation features in quartz while K-feldspar usually shows brittle deformation. The green aggregates have a

Table 1. *Mineralogical composition Iv1, Iv1b, Iv2*

Mineral	Vol %*	Vol %†
plagioclase	27	29
quartz	35	26
muscovite	15	17
garnet	4	5
K-feldspar	5	5
chlorite	6	6
clinozoisite	6	10
minor comp.	2	2

* By electron microprobe element mapping and phase analysis

† Average from Techmer (1996)

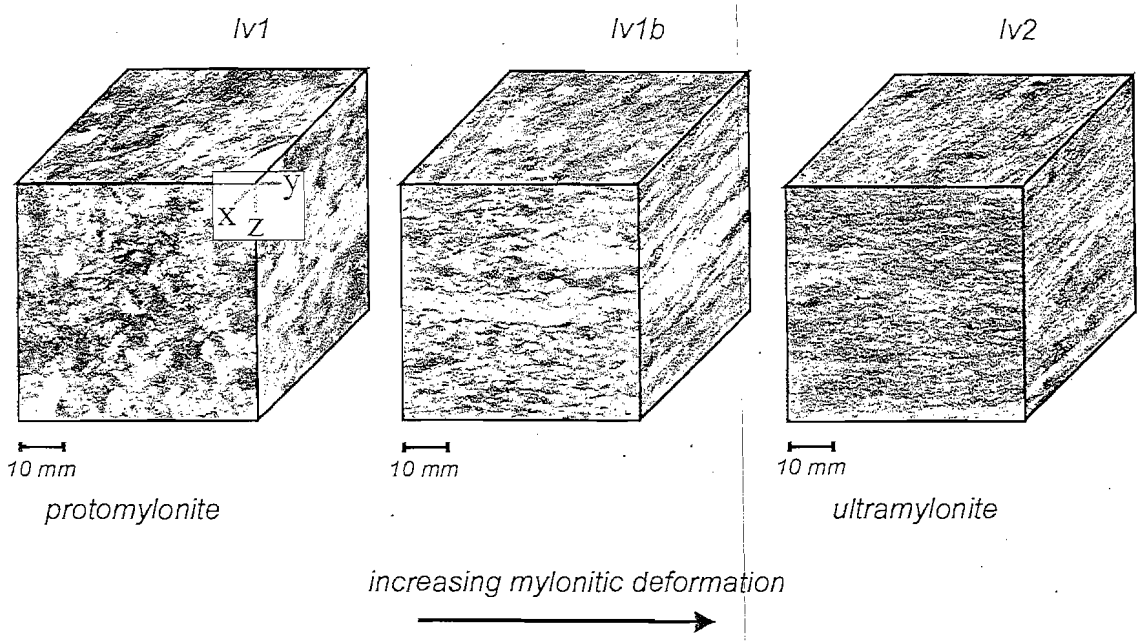

Fig. 2. Foliation development due to mylonitization. Scanned cubes. Dark layers are chlorite and clinozoisite/epidote enriched; bright layers are quartz and albite enriched.

diameter of 3–4 mm. Albite, chlorite and sericite as a part of these aggregates are fine-grained (about 1–2 μm). Within the rest of the material they show a grain size of 100–150 μm. As a result of the progressive mylonitic deformation Iv2 is dominated by an equigranular fabric with an intermediate grain size of 150–300 μm (Fig. 3). The occurrence of large quartz and feldspar grains decreases from Iv1 to Iv2. The microcrystalline aggregates suffer a strong flattening and are concentrated in distinct layers. The density of all the samples is 2.74 g cm^{-3} and the results of mercury porosimetry reveal a maximum of pore radii between 0.01 and 0.1 μm (Fig. 4).

Texture

From other research studies it is well known that the texture of the rock-forming minerals is a very important factor for physical and mechanical properties of the whole rock. The texture of muscovite as well as of quartz and albite were determined. The samples exhibit a pronounced quartz texture pattern; however, the intensity of the texture is low. Therefore the effect on the mechanical properties should be of minor importance. Albite has a weak texture (Fig. 5), and will therefore not be discussed in detail, whereas muscovite shows a pronounced texture. This associated with the high anisotropic properties and the mechanical weakness of the muscovite 001 plane leads to the assumption that muscovite controls the mechanical and physical properties (e.g. Shea & Kronenberg 1993; Siegesmund *et al.* 1995; Siegesmund 1996). The muscovite preferred orientation becomes stronger in the sample set with progressive mylonitization. Sample Iv1 reveals an approximately complete girdle distribution about the stretching lineation (x) with a maximum of (001) poles 30° inclined to the z-axis. Weakly developed girdles with a strong point maximum close to the foliation pole are evident in samples Iv1b and Iv2. The fabric symmetry becomes more oblate without reaching a perfect transversal isotropic pattern (Fig. 6a–c).

A well-established and frequently used method for the quantification of fabrics in a deformed rock is the determination of the anisotropy of the magnetic susceptibility (e.g. Hrouda 1982; Borradaile 1988; Siegesmund *et al.* 1995). In gneissic rocks, paramagnetic phyllosilicates with lattice-dependent magnetic properties are assumed to control the whole rock AMS which was quantitatively shown by Siegesmund *et al.* (1995). The only paramagnetic and anisotropic minerals in the Sesia-Lanzo mylonites are muscovite, chlorite and clinozoisite/epidote. The latter has only a weak anisotropy with respect to the magnetic properties, and may not have a great impact on the

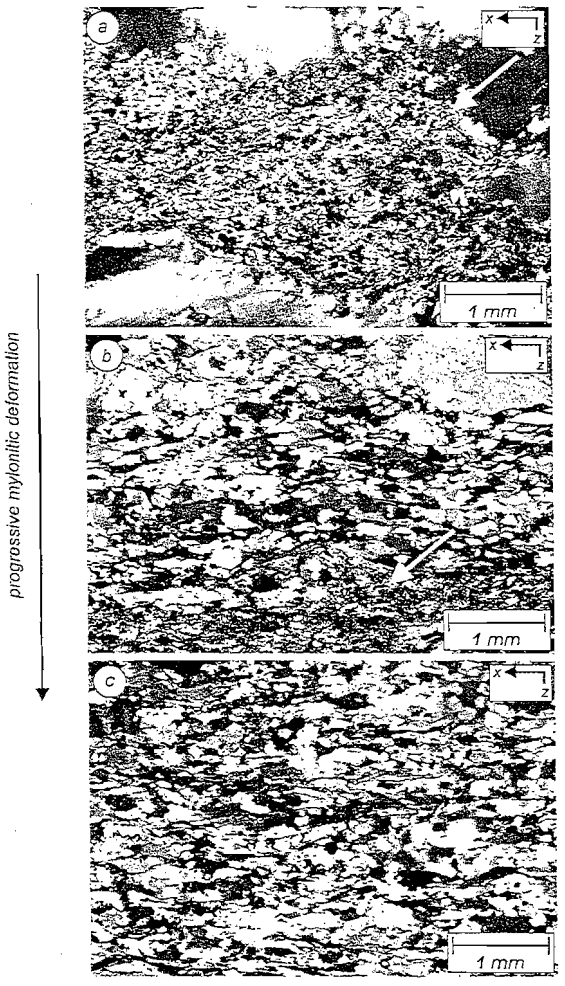

Fig. 3. Fabric development. Optical micrographs; crossed polarizers. Microcrystalline aggregates (see text) are marked by white arrows. (**a**) xz-plane of sample Iv1. (**b**) xz-plane of sample Iv1b. (**c**) xz-plane of Iv2.

Table 2. *Anisotropy of magnetic susceptibility data*

Sample	L	F	T	P	$P`$
Iv1	1.017	1.004	−0.635	1.021	1.023
Iv1b	1.027	1.050	0.335	1.079	1.080
Iv2	1.015	1.037	0.667	1.052	1.054

L, lineation factor after Balsey and Buddington (1960); F, foliation factor after Stacey *et al.* (1961); T, shape factor after Jelinek (1981); P, factor of anisotropy after Nagata (1961); $P`$, factor of anisotropy after Jelinek (1981)

bulk rock magnetic susceptibility. Muscovite and chlorite, which are highly anisotropic, may influence the magnetic properties in the same way because of their similar magnetic behaviour (Borradaile 1987).

K_{max} of the AMS ellipsiod is aligned parallel to the stretching lineation (x), whereas K_{min} is subparallel to the maximum of muscovite (001) poles (for the AMS data see Table 2). K_{int} lies perpendicular to the lineation within the foliation. This holds true for all three samples (Fig. 6a–c) and mainly coincides with observations made by Juckenack (1990) and Siegesmund *et al.* (1995). The length of the half axes of the AMS ellipsoid increases from Iv1 to Iv2. The shape factor T (Jelinek 1981) covers the range from −0.635 corresponding to a more prolate AMS ellipsoid to a highly oblate AMS ellipsoid with values of 0.667 (Fig. 7).

Microcracks

The samples Iv1b and Iv2 display an approximately orthogonal microcrack pattern which is nearly orientated perpendicular to the axis of the reference system and parallel to the xy-, yz- and xz-planes, respectively. The microcrack pattern of Iv1 is comparable to that of the other two samples, however Iv1 is rotated 30° around the x-axis (Fig. 8a). The main features of the whole microcrack families are intragranular

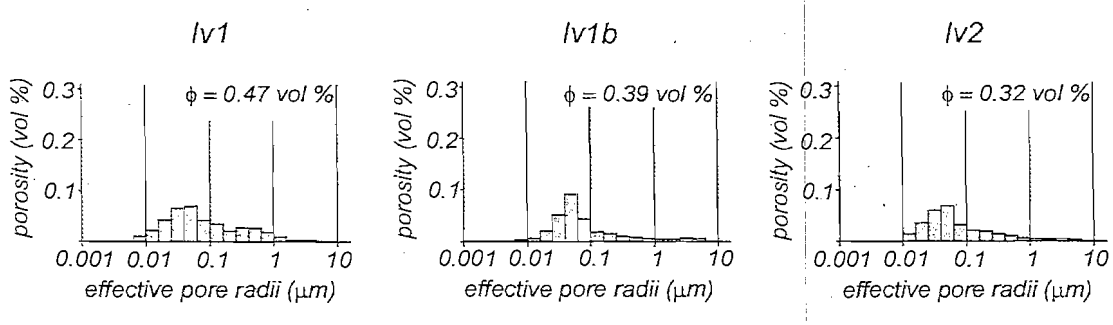

Fig. 4. Pore radii distribution. Φ is total porosity.

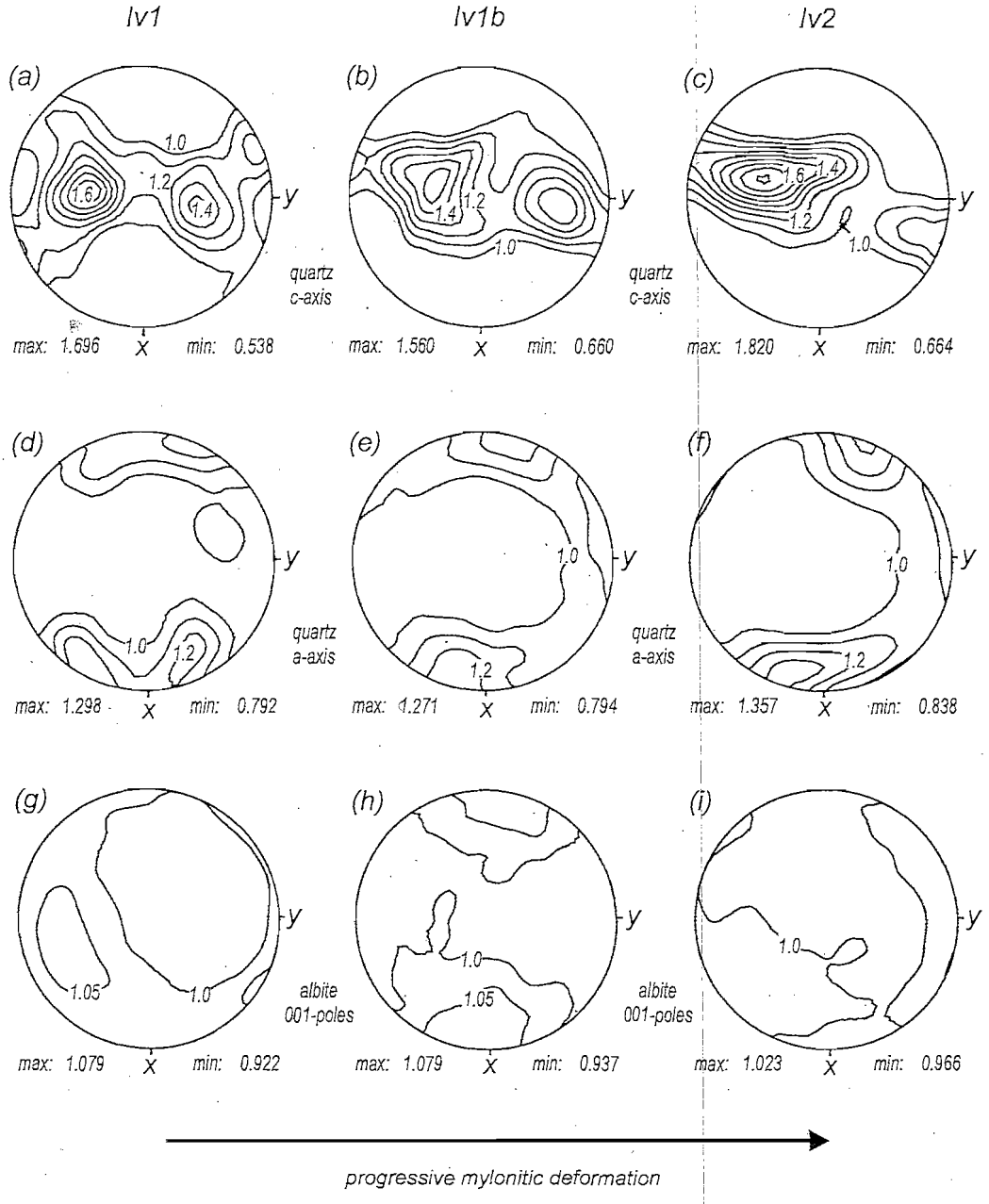

Fig. 5. Quartz and albite texture. Schmidt-net lower hemisphere; multiples of random distribution. (**a–c**) Distribution of quartz c-axis. (**d–f**) Distribution of quartz a-axis. (**g–i**) Distribution of albite (001) poles.

healed, open, mineralized and cleavage cracks (for nomenclature see Kranz 1983; Vollbrecht *et al.* 1994). The cleavage cracks frequently occur parallel to the (001) plane of muscovite and chlorite (Fig. 8b). Quartz accommodates a great amount of healed cracks decorated with secondary fluid inclusions, which occur most frequently parallel to the yz-plane (Fig. 8c). Open and mineralized cracks displaying a more irregular shape can also be observed in quartz but less often (Fig. 8d). K-feldspar, clinozoisite/epidote and garnet exhibit open and irregular-shaped microcracks (Fig. 8e). Progressive mylonitization causes changes in the microcrack system. The development of a stronger phyllosilicate texture leads to a more preferred orientation of (001) cleavage cracks from the protolith (Iv1) to the ultramylonite (Iv2). Dynamic recrystallization is another process that influences the microcracks in quartz and albite leading to a

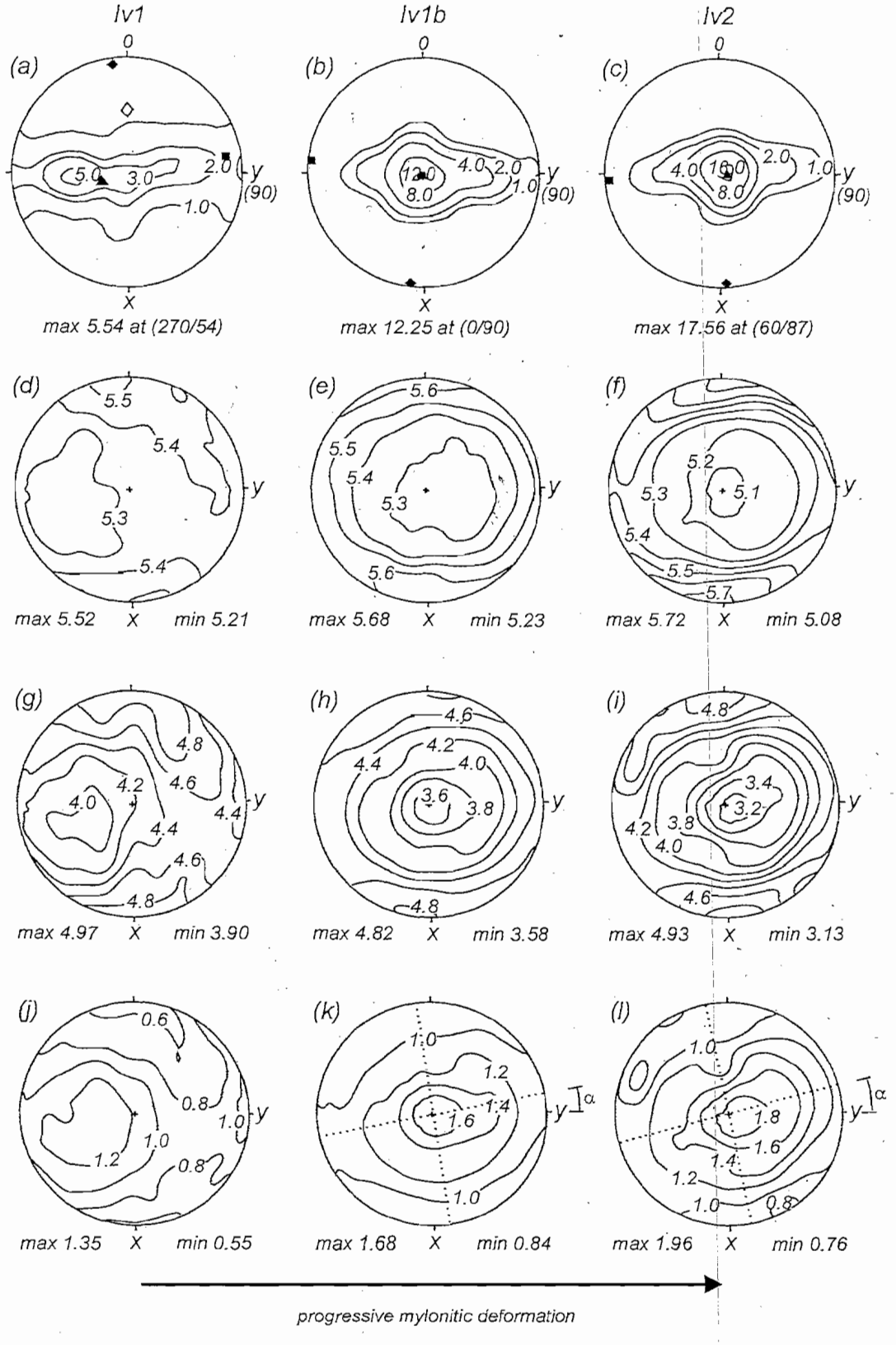

Fig. 6. Muscovite texture and compressional wave velocities. (**a–c**) Muscovite (001) poles in multiples of random distribution (220 grains per sample); main axis of AMS ellipsoid: K_{max} (rhombes); K_{int} (squares); K_{min} (triangles). (**d–f**) Vp (km s^{-1}) pattern of the water-saturated spherical specimens. (**g–i**) Vp (km s^{-1}) pattern of dry spherical samples. (**j–l**) Calculated ΔVp pattern (Vp of saturated sample minus Vp of dry sample); dotted lines show estimated maxima of planes of microcrack systems excluding the muscovite cleavage planes. Estimates of Vp experimental error are ± 50 m s^{-1}.

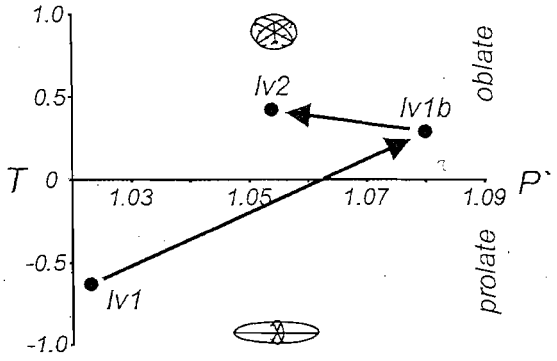

Fig. 7. P`–T diagram after Jelinek (1981).

reduction of pre-existing microcracks (Passchier & Trouw 1996). Furthermore the loss in grain size leads to shorter cracks (Iv1b, Iv2) in contrast to those described in Iv1. In summary, the mylonitic deformation accomplishes a concentration of (001) phyllosilicate cleavage cracks and a loss in healed and mineralized cracks in quartz and albite including smaller crack length. The cleavage cracks become more dominant from Iv1 to Iv2.

To quantify the different microcrack populations and their orientation the analyses of the compressional wave velocities can be applied (see Experimental section).

The maximum of open microcrack poles marked by the highest ΔVp in the diagram (Fig. 6j–l) coincides with the maximum of muscovite (001) poles. Hence, it can be concluded that muscovite cleavage cracks are the most dominant crack population. The contribution of other cracks to the ΔVp pattern is more complicated. The coincidence of the orthogonal microcrack pattern (see Fig. 8a) with the orthogonal *Vp* pattern (Fig. 6k–l) is probably a first indication. This cannot be explained by the muscovite texture alone (see Fig. 6a–c). The significantly higher *Vp* of the cylindrical specimen under a confining pressure of 400 MPa in comparison to the *Vp* of the water-saturated samples obtained along the same directions (Table 3) clearly documented that the crack porosity and the trapped pore space have their influence on the *Vp* pattern, respectively. The distribution of healed cracks within the sample set are interpreted as potential planes of mechanical weakness. However, they cannot be estimated by this approach.

Mechanical properties

Tensile strength

The tensile strength covers the range of 7.7 to 19.3 MPa (Table 4) for all investigated samples and directions (x-, y- and z-direction means direction of tensile forces is parallel to the x-, y- and z-axis of the reference system; see Fig. 1). In all samples the z-direction reveals the lowest and the x-direction the highest strength values, whereas the y-direction is intermediate (Fig. 9). With the mylonitization the anisotropy ([strength max. minus strength min.]/strength max.) of the tensile strength increases from 26% (Iv1) to 48% (Iv1b) and finally to 60% (Iv2). The x-direction becomes higher in strength, whereas the z-direction becomes less pronounced. The y-direction is more or less constant. During the indirect tensile strength

Table 3. *Ultrasonic wave velocities*

Sample*	*Vp*, 2 MPa† (km s^{-1})	*Vp*, 400 MPa† (km s^{-1})	*Vp* saturated‡ (km s^{-1})	*Vp* 400 MPa – *Vp* saturated (km s^{-1})
Iv1x	4.87	6.42	5.49	0.93
Iv1y	4.14	6.31	5.39	0.92
Iv1z	4.42	6.24	5.35	0.89
Iv1bx	5.11	6.67	5.66	1.01
Iv1by	4.65	6.30	5.53	0.77
Iv1bz	3.63	6.11	5.25	0.86
Iv2x	5.26	6.69	5.72	0.97
Iv2y	4.40	6.33	5.39	0.94
Iv2z	3.31	6.05	5.10	0.95

* x, y, z indicate velocities parallel to x, y or z axis
† Derived from measurements of dry cylindrical samples under a confining pressure
‡ Derived from measurements of water-saturated spherical samples

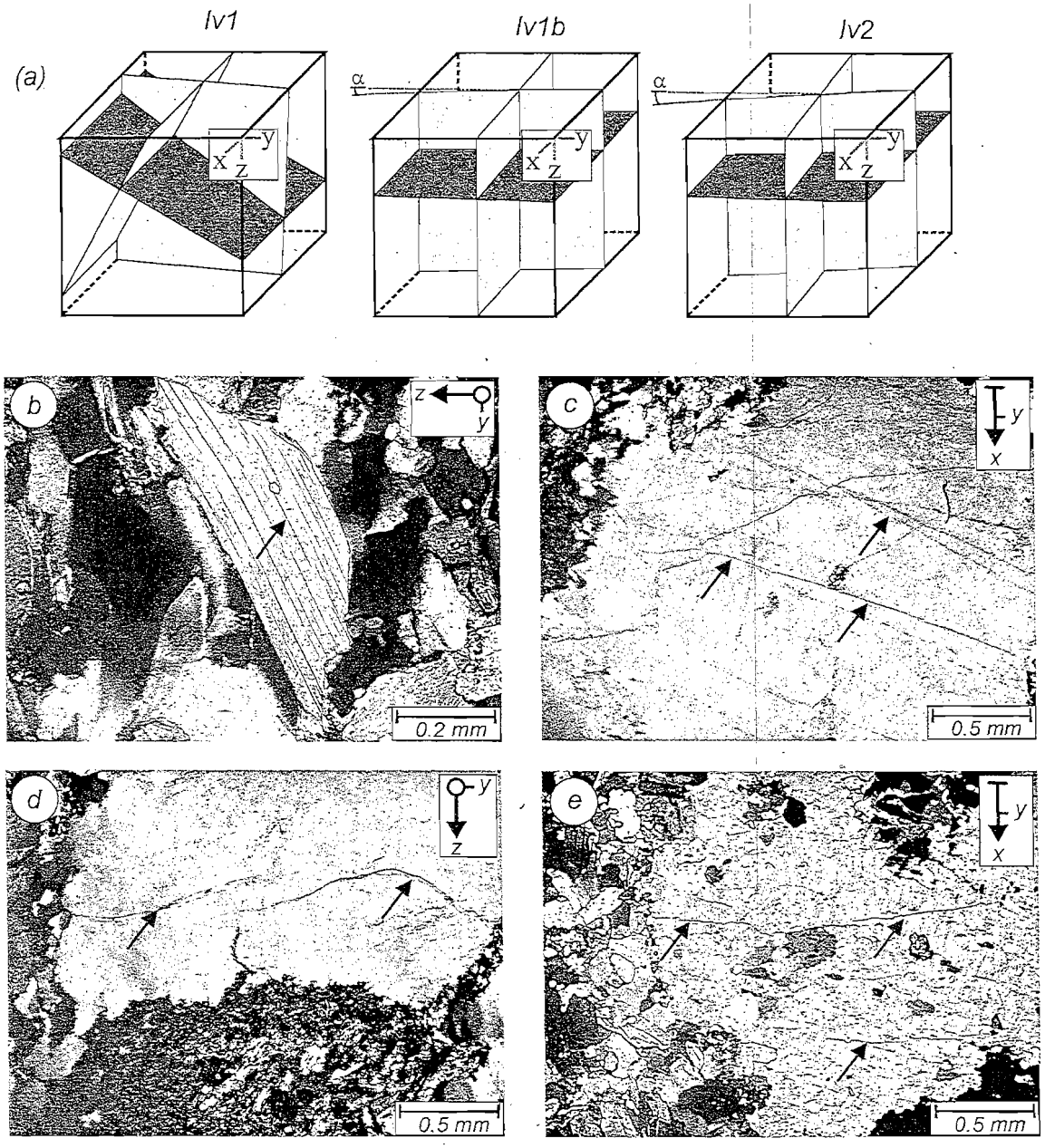

Fig. 8. Pre-existing microcracks. Optical micrographs; crossed polarizers (**a**) Orientation of microcrack systems in Iv1, Iv1b and Iv2; dark grey planes mark the preferred orientation of muscovite (001) cleavage planes. (**b**) Open cleavage cracks in muscovite; example marked by arrow (sample Iv1b). (**c**) Healed microcracks decorated with secondary fluid inclusions; examples marked by arrows (sample Iv1). (**d**) Mineralized microcracks in quartz marked by arrows (sample Iv1). (**e**) Open microcracks in K-feldspar; examples marked by arrows (sample Iv1b).

test (Brazilian test), the specimens fail if the stress exceeds the cohesion of the starting material (Nagaraj 1993). To investigate the fracture plane in more detail the scanning electron microscope was applied. In most cases the muscovite cleavage planes are the planes of weakness and often get activated during failure (Fig. 10a). In particular, the z-direction seems to be weak because of the strong muscovite texture causing a preferred orientation of (001) planes parallel to the xy-plane. Albite and K-feldspar also fail along their cleavage planes (Fig. 10b). Moreover, microcrack formations along interconnected microcrack networks can

Fig. 9. Compressive and tensile strength. Tensile strength values and twice standard deviation within grey rectangles; compressive strength and twice standard deviation within cylinders; direction of compressive and tensile forces marked by arrows; schematic prefered orientation of muscovite marked by black bars inside the cubes.

Table 4. *Mechanical properties*

Sample*	Tensile strength† (MPa)	Number of measured samples	Compressive strength‡ (MPa)	Number of measured samples	Abrasive strength§ (cm^3)	Number of measured samples
Iv1x	13.5 (1.4)	6	221 (11)	5	7.36 (0.33)	2
Iv1y	11.1 (1.2)	5	201 (7)	5	7.58 (0.17)	2
Iv1z	10.0 (1.5)	8	206 (3)	5	8.58 (0.20)	3
Iv1bx	18.3 (0.7)	5	225 (56)	9	6.81 (0.21)	2
Iv1by	12.6 (1.5)	9	128 (26)	5	7.93 (0.30)	2
Iv1bz	9.5 (1.5)	18	168 (35)	5	8.87 (0.27)	2
Iv2x	19.3 (1.1)	6	200 (27)	7	6.40 (0.14)	3
Iv2y	12.5 (1.4)	17	155 (22)	5	7.91 (0.23)	3
Iv2z	7.7 (1.1)	14	172 (20)	8	9.14 (0.22)	2

* x, y, z indicate strength parallel to x, y, z axis or plane perpendicular to x, y, z axis (Boehme method)
† Determined by Brazilian test following the recommendations of DIN 22024; numbers in brackets are twice standard deviation
‡ Determined by uniaxial compression test following the recommendations of DIN EN 1926; numbers in brackets are twice standard deviation
§ Determined by Boehme test following the recommendations of DIN 52108; numbers in brackets are twice standard deviation

be clearly documented in Figure 10c,d. Grain boundaries are also zones of weakness (Fig. 10e). Less than 10% in total of the fracture surface is estimated as grain boundaries. The fracture zones are related to newly formed open and reactivated pre-existing, mineralized and healed cracks. The nucleation and propagation of mode-I (tensile) transgranular cracks favourably follow the cleavage planes of the rock-forming minerals.

Uniaxial compressive strength

The uniaxial compressive strength (UCS) ranges between 225 MPa and 128 MPa (Table 4) (x-, y- and z-direction means direction of load is parallel to x-, y- and z-axis of the reference system; see Fig. 1). Due to the progressive mylonitization among the sample set, the UCS values exhibit no distinct development (Fig. 9). Sample Iv1 is approximately isotropic (concerning the determined directions) whereas Iv1b is the most anisotropic one (43%). The x-direction in the case of Iv1b and Iv2 exhibits the highest (225 MPa and 200 MPa, respectively), whereas the y-direction shows the lowest UCS values (128 MPa and 155 MPa, respectively). The results of optical investigations reveal that in uniaxial compression tests, the cleavage planes of the rock-forming minerals and pre-existing microcracks were activated by propagation of mode-I (tensile) and mode-II (shear) crack pairs. The influence of open grain boundaries is of minor importance. The failure pattern varies significantly with regards to the progressive mylonitization. Most conspicuous is the x-direction. Iv1 samples exhibit a cone-shaped fracture plane, whereas Iv1b shows a roof-shaped appearance. The fracture pattern of Iv2 tends to be a roof-shaped form, but is not as distinct as in Iv1b and comprises kinking of the foliation (quartz-albite-enriched and chlorite-clinozoisite/epidote-enriched layers) and macroscopical splitting parallel to the foliation plane (Fig. 11a–d). The pattern of failure planes in the y- and z-direction are always roof-shaped but the geometrical form of the fracture planes becomes more distinct from Iv1 to Iv2. All fracture planes reveal a facet-like geometry and a certain bowed shape according to the shear stress distribution within the specimen (Fig. 12). Stress–strain diagrams are generated and displayed in Figure 13. The general behaviour of the samples is similar in all directions. Nevertheless, the data suggest that samples bearing high compressive strength values tend to show a steeper slope coinciding with a higher compression modulus (for example Iv1b, x-direction) and vice versa (for example Iv1b, y-direction).

Abrasive strength (Boehme method)

The Boehme values (known as abrasive strength) vary between 6.40 cm^3 and 9.14 cm^3 (Table 4). For the Boehme method the x-, y-, z-direction corresponds to the planes orientated perpendicular to the x, y, z-axis of the reference system (see Figs 1 and 14). Lower values are

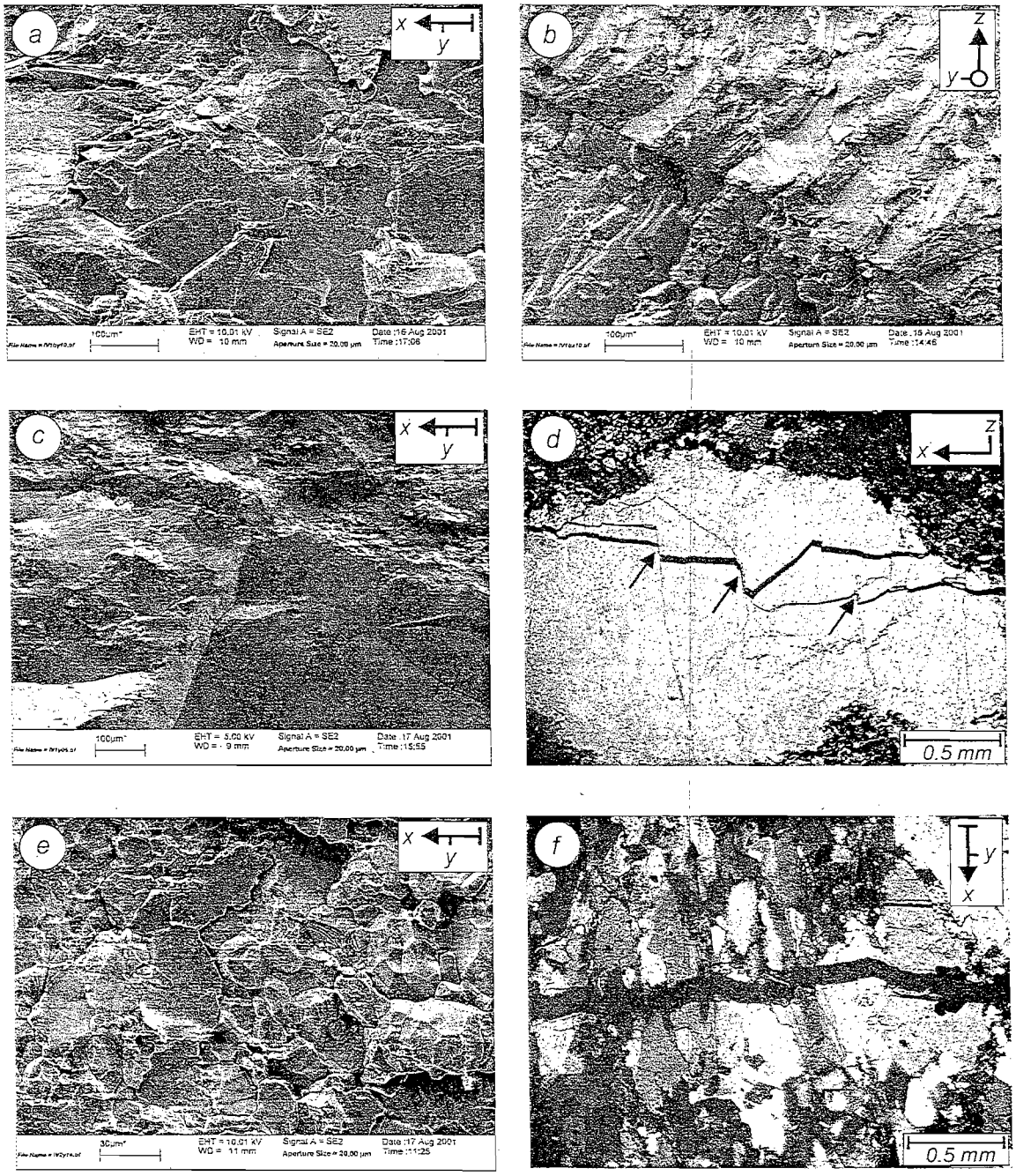

Fig. 10. Favourably activated planes in Brazilian test. Scanning electron micographs; secondary electrons (a–c, e) and optical micrographs; crossed polarizers (d, f). (**a**) Activated (001) plane in muscovite. (**b**) Fracture of K-feldspar (baveno-twin); (001) and (010) cleavage planes activated. (**c**) Activated healed microcrack in quartz. (**d**) Activated healed microcracks in quartz marked by arrows. (**e**) Fracture pattern in microcrystalline quartzitic area. (**f**) Fracture plane filled by resin in sample Iv1b.

attributed to high abrasive resistance and vice versa. The anisotropy of the individual samples increases from Iv1 (14%) to Iv2 (30%) (Fig. 14). The highest abrasive strength is observed for the x-direction while the z-direction is consistently lower. This holds true for all three samples. The increasing mylonitic deformation leads to a stronger x-direction and a weaker z-direction (Fig. 14). The y-direction is invariant. No indication of SiC (abrasive used in the

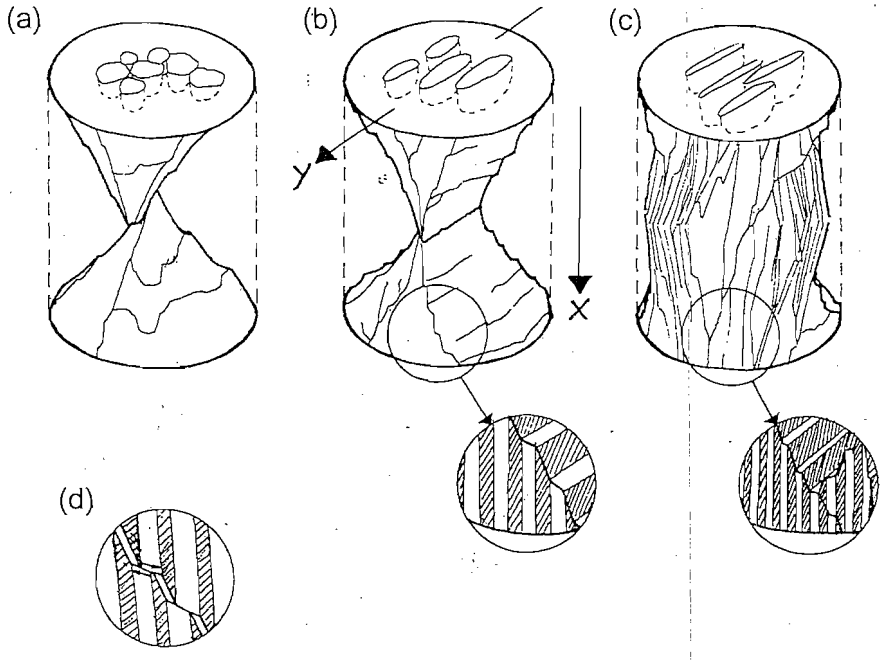

Fig. 11. Fracture pattern after uniaxial compression test. Samples cored and tested parallel to the x-direction. The x- and y-axes of the reference system are indicated in (b). (**a**) Iv1. (**b**) Iv1b. (**c**) Iv2. (**d**) Crack propagation during uniaxial compression test; arrows mark dislocation direction.

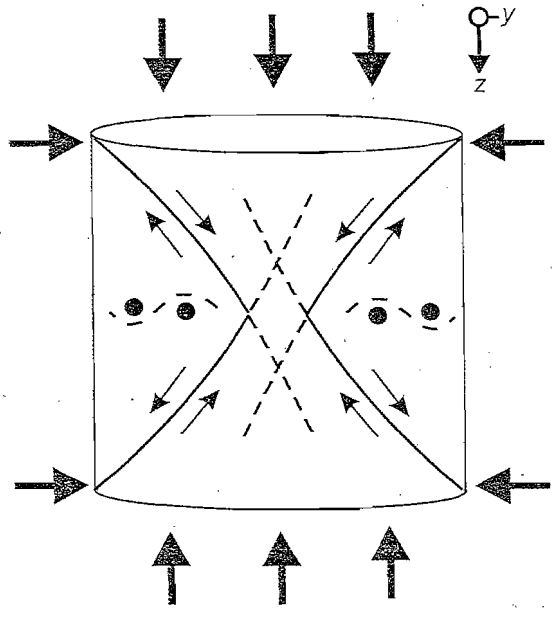

Fig. 12. Uniaxial compression test. Direction of sample load and forces at top and bottom of the sample (bold arrows); black lines mark planes of maximum shear stress; shear sense indicated by small arrows.

Boehme test) traces can be observed on the surfaces of the tested samples. The sample surfaces are rough and the abrasion seems to be controlled by mineral destruction processes. For the progressive abrasion muscovite basal planes (Fig. 15a,b), albite and K-feldspar cleavage planes as well as pre-existing microcracks were preferrentially activated (Fig. 15c,d). Therefore, abrasive strength does not only depend on the Mohr hardness of the rock-forming minerals, but on the abundance and interlocking of minerals and pre-existing microcracks and their preferred orientation. Activation of grain boundaries is of minor importance and is rarely observed in the tested samples.

Discussion

Until recently several attempts have been made to quantify the relation between rock fabric and mechanical properties. Howarth & Rowlands (1987) calculated a texture coefficient (TC) considering a wealth of fabric parameters like grain size, grain shape, packing density, porosity and degree of interlocking. However, the results suggest that the TC is only sufficient as a pre-predictive tool and does not provide precise results (Ersoy & Waller 1995; Azzoni *et al.* 1996). For example, in metamorphic rocks the predicted mechanical properties constrained by the TC do not show a good agreement with the experimental data (Brosch *et al.* 2000).

This study has focused on the fabric development in a progressively mylonitized sample set

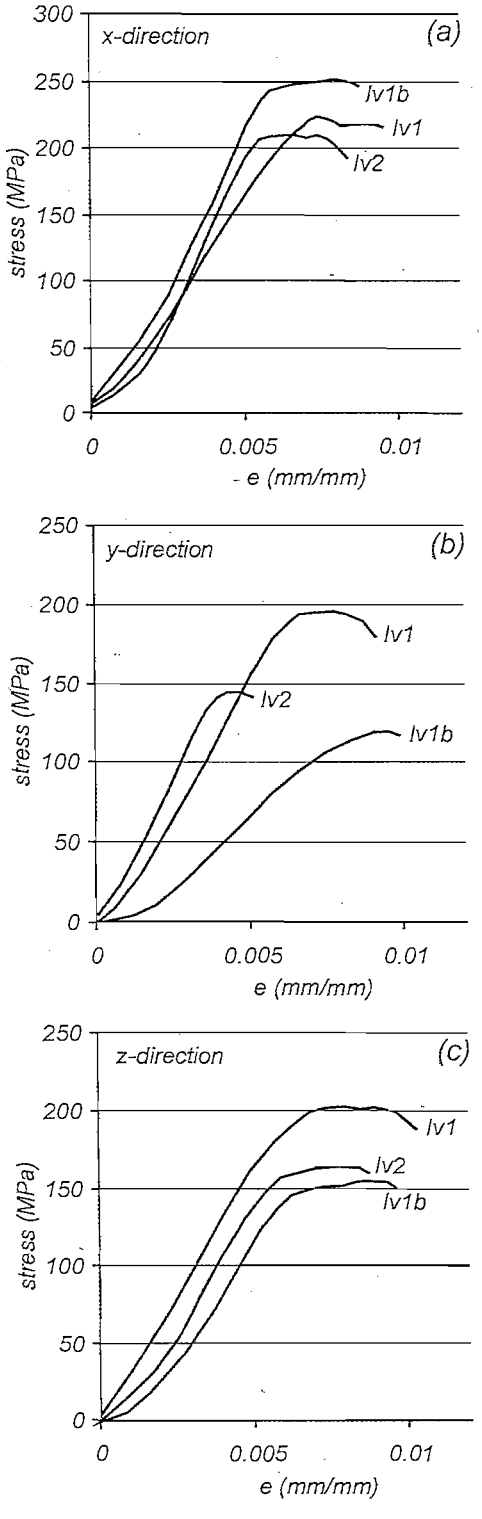

Fig. 13. Stress–strain curves derived by uniaxial compression test.

and its control of the physical and mechanical rock properties. The solid state behaviour of well-foliated rocks depends on the rheology and the volume content of the weakest mineral, forming continuous layers in favourable orientation (Jordan 1988; Handy 1990; Shea & Kronenberg 1992, 1993).

The phyllosilicates show a perfect cleavage parallel to their (001) plane and often exhibit a strong preferred orientation in metamorphic rocks. They are the weakest component in the rock with respect to their strength (as observed by Muegge 1898). They are assumed to control the rock strength (Gottschalk *et al.* 1990; Shea & Kronenberg 1993). Biotite and muscovite exhibit relatively low activation energies for dislocation of 82 kJ mol^{-1} (Kronenberg *et al.* 1990) and 47 kJ mol^{-1} (Mares & Kronenberg 1993), respectively, in comparison to stronger silicates like plagioclase with 237 kJ mol^{-1} (Shelton 1981; Tullis *et al.* 1991). The strong textures observed in phyllosilicates like muscovite and chlorite are accompanied by a high anisotropic mechanical behaviour (Kronenberg *et al.* 1990) which probably is responsible for the anisotropic mechanical rock properties.

Concerning the compressive strength the proportional number of mica grains aligned for sliding (parallel to (001) plane) and kinking has a great impact on the rock strength. High contents lead to relatively lower compressive strength values, but the volume content and the mica subfabric are important factors too. If the micas build interlayers a great amount of stress that occurs will get resolved on the (001) planes by sliding. This, coinciding with volume contents higher than 30%, leads to a ductile response (easy glide; Christoffersen & Kronenberg 1993). A more randomly preferred orientation and a dispersed arrangement of mica within a framework of other rock constituents like feldspar and quartz cause a more brittle response due to compressive forces. This includes crack nucleation and crack propagation of mode-I flaws within the brittle silicate framework due to mode-II crack (frictional sliding parallel to mica (001) planes) interaction (Segall & Pollard 1980; Gottschalk *et al.* 1990; Shea & Kronenberg 1993).

Considering the tensile strength, the volume percentage of phyllosilicates (001) planes orientated with angles near 90° to tensile forces is of great importance (Peck *et al.* 1985). High mica contents cause relatively lower resistance of rock to tensile fracture. However, other factors may contribute to rock strength. For example pre-existing sets of microcracks and the

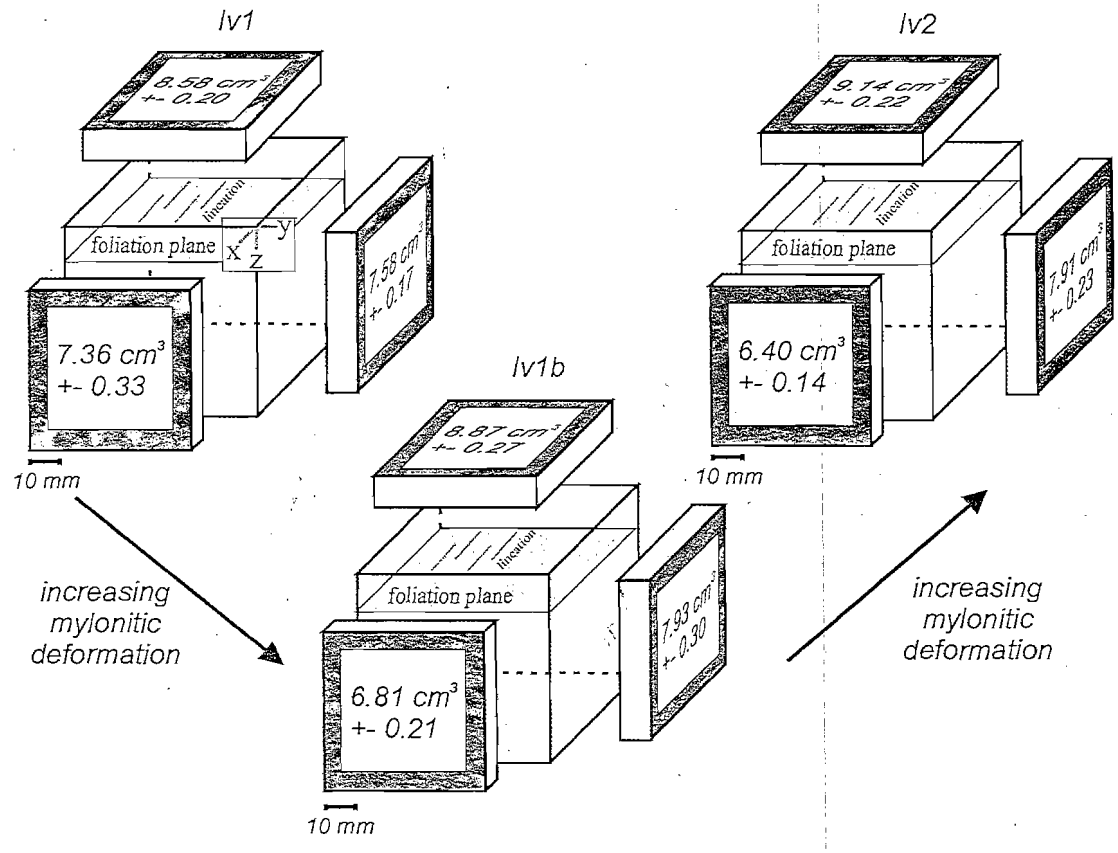

Fig. 14. Abrasive strength; given volumes indicate material loss.

feldspars with their perfect cleavage parallel to the (001) plane are assumed to influence the tensile and compressive strength values (Peck *et al.* 1985; Gottschalk *et al.* 1990; Li *et al.* 1998). Pre-existing microcracks in many cases follow crystallographic planes (Vollbrecht *et al.* 1999). Hence, microcracks in phyllosilicates tend to occur parallel to the (001) plane and intensify the effect of phyllosilicate texture.

Phyllosilicates dominate the physical and mechanical properties of a rock. Therefore, the strength data will be compared to the muscovite distribution pattern and the resulting symmetry of the AMS tensor. If indeed the tensile strength and abrasive strength of the examined rocks mainly depend on the muscovite texture, their development from a prolate (Iv1) to a more oblate fabric (Iv1b and Iv2) should cause similar symmetries of the mechanical properties. Due to the muscovite preferred orientation the x- and y-directions should become more alike and the z-direction should develop weaker abrasive and tensile strength values. The latter is observable among the sample set, whereas the x-direction shows increasing strength values due to the progressive mylonitization and the y-direction is approximately constant (Fig. 16a,b). Hence, the symmetry of strength values does not become oblate. This cannot be explained by the mica lattice preferred orientation alone. Therefore, other fabric elements should be responsible for the observed strength variations parallel to the x-direction. Pre-existing healed microcracks accommodated in the large quartz crystals of Iv1 were reduced due to dynamic recrystallization processes, and therefore are less frequent in Iv1b and Iv2. This may cause the relatively higher strength values in the x-direction and in the plane perpendicular to the x-direction (Boehme method), respectively. A decrease in the proportional number of microcracks perpendicular to the x-direction should cause a relatively lower ΔVp parallel to the x-direction (Fig. 6). This is not observable among the sample set, since ΔVp values are approximately constant parallel to the x-direction (Fig. 16c). However, reactivated healed microcracks may be responsible for the change of strength parameters. As shown in Figure 10c,d, these certain microcracks often become activated during the Brazilian test and

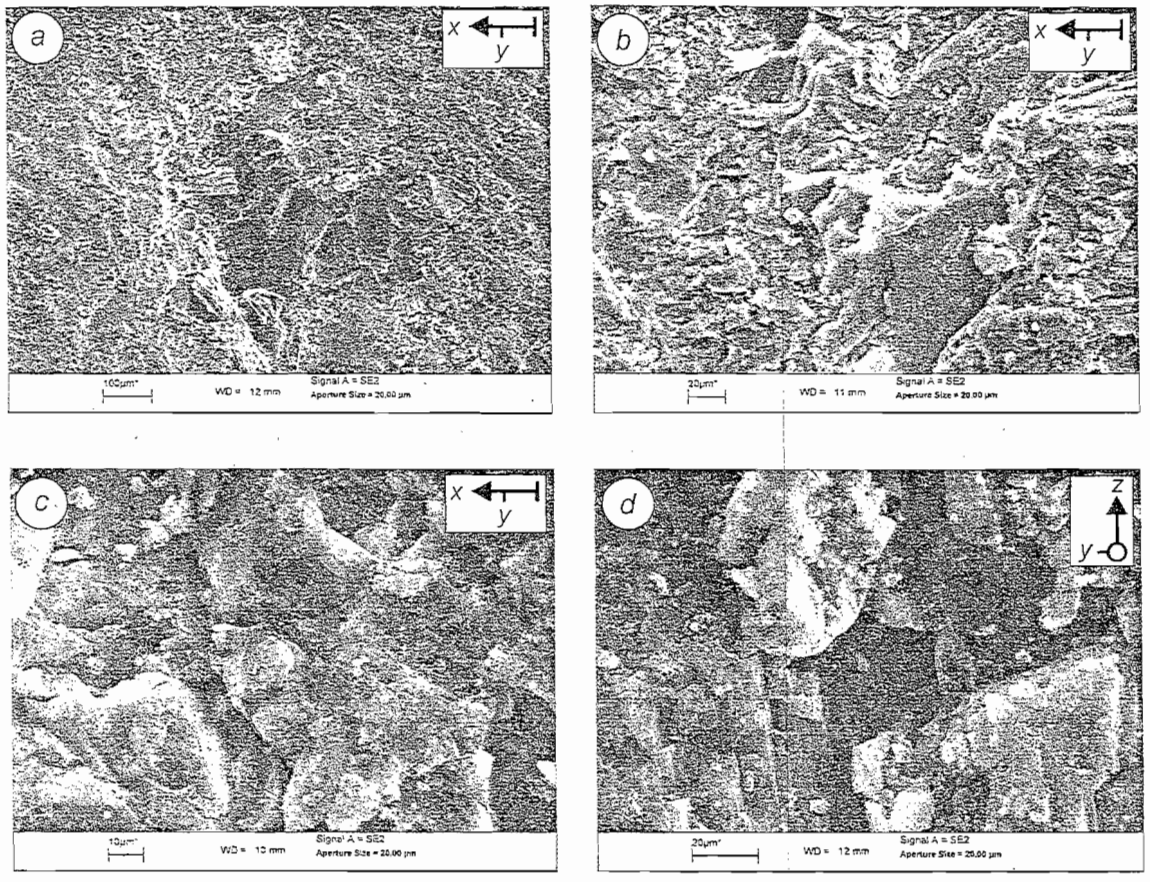

Fig. 15. Activated planes in Boehme test (abrasive test). Scanning electron micrographs; secondary electrons. (**a**, **b**) Activated (001) planes of muscovite. (**c**) Quartzitic area after the Boehme test. (**d**) Activated (001) and (010) planes in K-feldspar.

cause no significant changes in ΔVp pattern (see Experimental section).

Muscovite texture may to a great extent influence the tensile and abrasive strength values. This may be provided by a good direct correlation between the Vp_{sat} representing the intrinsic Vp and the strength values (Fig. 17a,b). However, a complete model predicting the rock strength and symmetry development due to fabric changes has to consider the distribution of microcracks and other parameters like grain size and development of any planar fabric, respectively.

The uniaxial compressive strength is an important and frequently used parameter to characterize the rock strength and has been investigated by several researchers. A few of these studies were performed to explain the rheology of the upper crust (e.g. Gottschalk *et al.* 1990; Shea & Kronenberg 1992, 1993) and others focused on geotechnical questions (e.g. Dearman *et al.* 1978; Koroneos *et al.* 1980; Schultz 1995; Duevel & Haimson 1997). In particular metamorphic rocks like gneisses show a strong directional dependency of compressive strength values. These rocks in many cases were assumed to be transversely isotropic with the foliation plane as an isotropic element. Even DIN EN 1926 recommends the determination of only two directions: the load perpendicular and parallel to any layering. Concerning the Sesia-Lanzo rocks the three measured directions reveal three varying compressive strength values in dependence of the fabric (Fig. 9).

The results of other investigations also exhibit varying compressive strength with respect to macroscopic fabric elements. Gottschalk *et al.* (1990) observed a maximum of compressive strength parallel to the macroscopic visible lineation. Brosch *et al.* (2000) found a maximum of UCS values perpendicular to the foliation plane, therefore perpendicular to the lineation. In the Sesia-Lanzo rocks the compressive

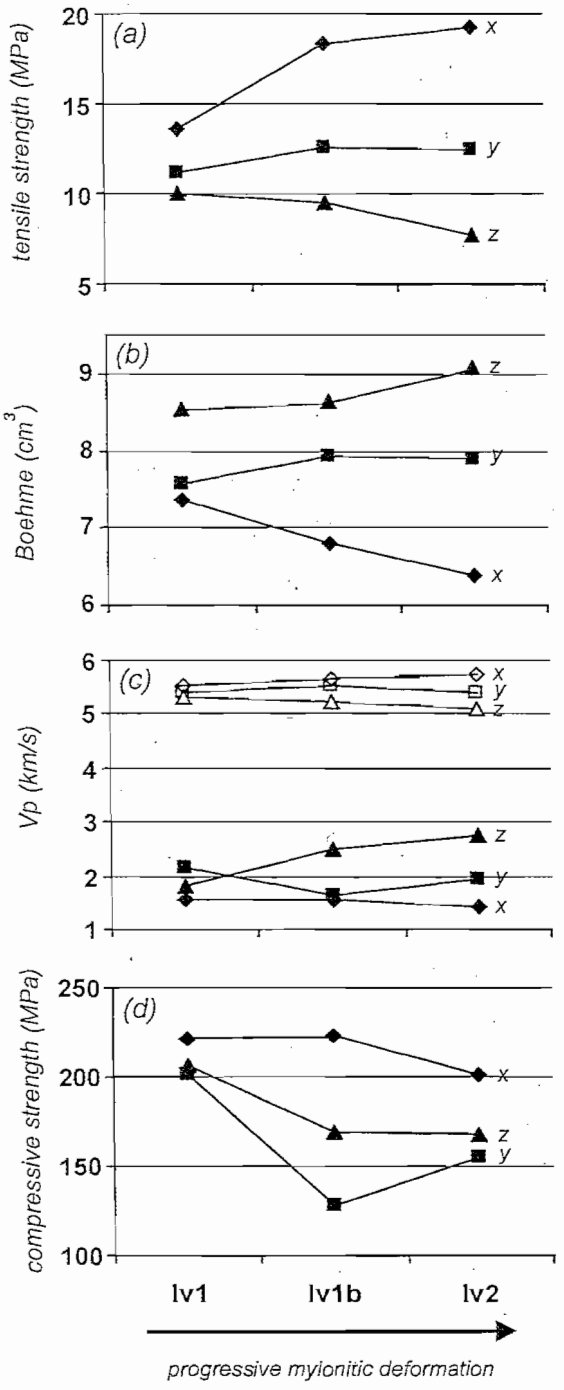

Fig. 16. Mechanical parameters and compressional wave velocities due to progressive mylonitization. The measured directions are indicated. (**a**) Tensile strength. (**b**) Abrasive strength (Boehme method); x-, y-, z-directions correspond to the planes perpendicular to the x-, y-, z-axes of the reference system. (**c**) Compressional wave velocities of water-saturated spherical samples (open symbols) and calculated ΔVp (bold symbols). (**d**) Compressive strength.

strength is highest in samples loaded parallel to the lineation. This holds true for the whole investigated sequence. When the development of mica texture is due to progressive mylonitization, the symmetry of compressive strength should be transformed from prolate to more oblate. The x-direction and the y-direction should reach similar values, whereas the z-direction is assumed to get the highest compressive strength. This is not valid in the case of the Sesia-Lanzo rocks (Fig. 16d). From Iv1b to Iv2 the predicted development is in part observable, but the prolate component remains dominant meaning the x-direction is the strongest direction. Between Iv1 and Iv1b the change of compressive strength does not fit to the model mentioned above. Instead of getting stronger the z-direction becomes weaker as well as the y-direction, whereas the x-direction is strongest and nearly constant (Fig. 9). This may be explained by the model of 'supply of planes of weakness' (planes of weakness defined as any plane of discontinuity within the rock sample; e.g. cleavage planes, foliation planes, layering, microcracks) and the particular stress localization during uniaxial compression. The diameter:length ratio of 1:1 as well as the interlocking of the ground sample and the ground loading plates of the universal testing machine cause 'quasi' triaxial conditions (Nagaraj 1993) and a particular location of shear stress among the specimen (Fig. 12). Slip planes may occur in angles of 18–45° to the direction of load (Stavrogin & Tarasov 2001). Hence, diameter:length ratios of 1:2 or even smaller may give different results. In DIN EN 1926 sample dimensions of 1:1 are recommended, with special emphasis on dimension stones. The orientation of planes of weakness at shallower angles with respect to shear stress influence the uniaxial compressive strength. If these planes are higher in concentration, a relatively lower compressive strength is expected and vice versa. The phyllosilicates and their texture have a great impact on the UCS values. The anisotropy within one sample (for example Iv1) can be explained by the influence of muscovite (001) planes and their related cleavage cracks orientated parallel to the planes of maximum shear stress.

Furthermore the layering, defined by quartz and albite, clinozoisite/epidote and chlorite layers, also controls the mechanical behaviour. A combination of mode-I (tensile) and mode-II (shear) cracks leads to a stepped geometry of the fracture plane (Stavrogin & Tarasov 2001) (Fig. 11a–d). The interlocking of both layers supported by the phyllosilicate content and distribution is also important. This is

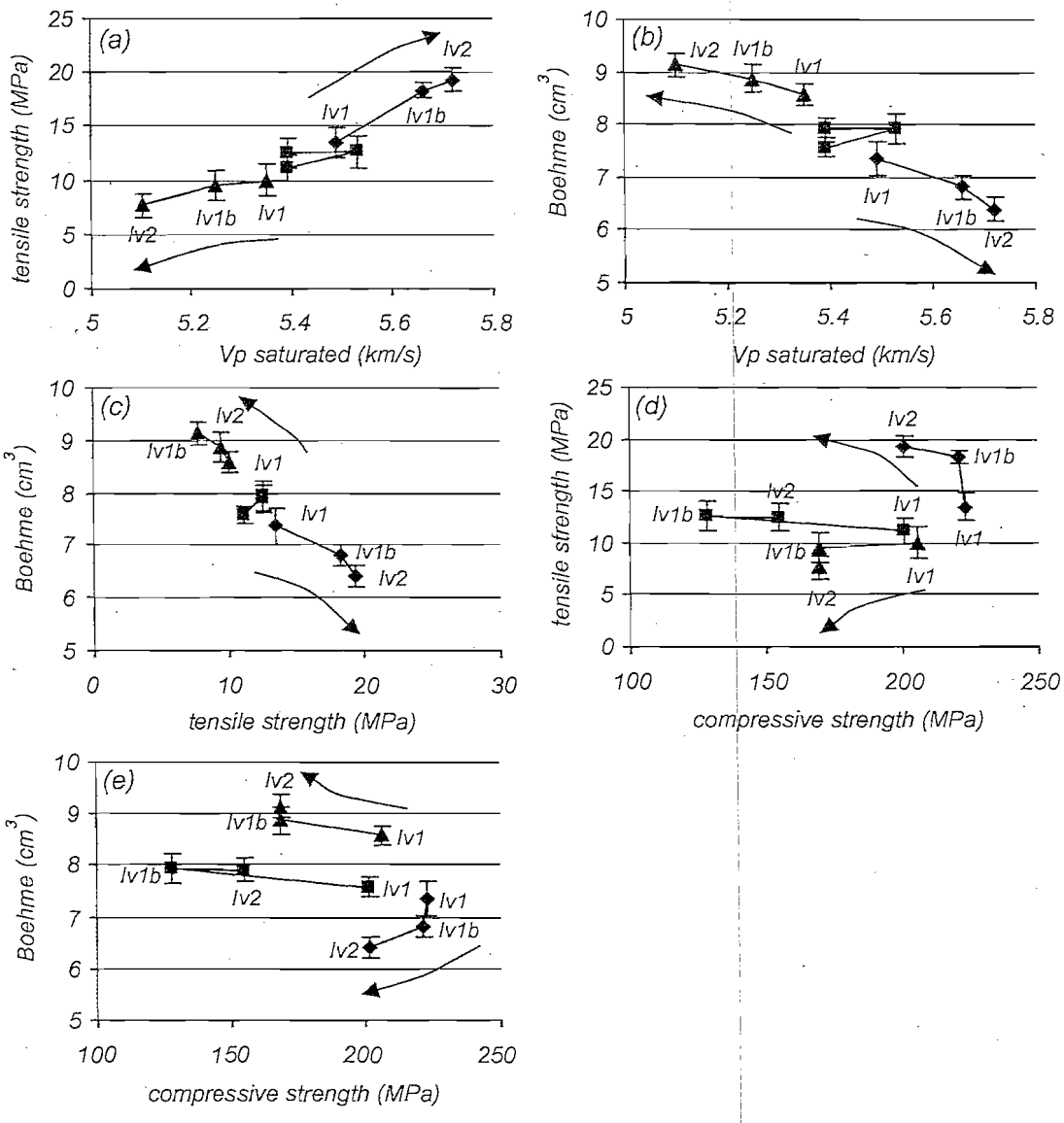

Fig. 17. Relations between mechanical and seismic parameters. The x-direction is marked by rhombes; y-direction marked by squares; z-direction marked by triangles; arrows display development of values due to progressive mylonitization. Experimental errors of compressive strength (d, e) see Table 4. For details see text.

clearly documented by the observed failure pattern of samples Iv1, Iv1b and Iv2 (Fig. 11a–c). For example in Iv2 loaded in the x-direction macroscopically visible mode-I cracks can be recognized. They do not occur in the samples Iv1 and Iv1b and can be explained by an improved fissility parallel to the foliation plane.

From Iv1 to Iv2 the increasing mylonitization leads to more narrowly spaced foliation, and therefore, should enhance the significantly lower strength in the y-direction.

Pre-existing microcracks accommodated by quartz and K-feldspar are not assumed to contribute greatly to compressive strength. In Iv1 the maxima of these microcrack systems (Fig. 8) are aligned to weaken the y- and z-direction of the load. Despite this fact, these directions exhibit the highest compressive strength values considering all samples.

In summary, the conditions during a uniaxial compression test are more complex than in the tensile strength test and Boehme method. The direction of the shear forces does not coincide with the direction of sample load. The interlocking of the sample and the testing machine

makes the stress location triaxial (Fig. 12). Hence, it is not possible to explain the development of UCS values due to progressive mylonitization in detail.

Conclusions

Tensile and abrasive strength mainly depend on the preferred orientation of phyllosilicates (e.g. muscovite) and their related microcracks. In detail other sets of microcracks like healed or mineralized cracks have to be taken into account. Consequently, the development of fabric, in particular of the phyllosilicate texture, causes changes concerning the tensile and abrasive strength. The tested specimens fractured by nucleation and propagation of mode-I cracks along cleavage planes of rock-forming minerals and pre-existing microcracks.

The development of compressive strength values cannot be explained adequately by changes of phyllosilicate texture. Other factors like grain size reduction, more closely spaced foliation, segregation in layers composed of quartz/albite or clinozoisite/epidote/chlorite and increasing fissility parallel to the foliation plane may influence the compressive strength. All these superimposed fabrics cause difficulties in discriminating the parameters (single fabric elements; planar or linear) which influence the rock strength. The quantity and spatial arrangement of discontinuities forming zones of weakness characterize the resistance of rock to compressive fracture.

Compressional wave velocity measurements on dry and water-saturated spheres are suitable for quantifying the crack-induced anisotropy in order to predict qualitatively the anisotropy of mechanical properties (Figs 6 and 17a,b).

Mechanical parameters which depend on similar failure processes (tensile and abrasive strength) exhibit a rather good direct correlation (Fig. 17c). Inspection of Figure 17d,e reveals that there are no distinct relations between the compressive strength on the one hand, and tensile and abrasive strength on the other hand. This may be caused by superimposing parameters and the fact that the direction of load does not coincide with the direction of maximum shear stress leading to sample failure due to uniaxial compression (see section on Uniaxial compressive strength). Moreover, the failure process during the compression test depends on the nucleation of mode-I and mode-II crack pairs (Fig. 11d) merged to form a macroscopic fracture plane in comparison to tensile and abrasive strength where only mode-I cracks occur.

The results of this study may be valid concerning the characterization of mechanical anisotropy of phyllosilicate-bearing rocks like gneisses and granites. For the purpose of applying these data to sedimentary rocks or rocks without any phyllosilicates further research work is necessary.

The authors thank the Bundesministerium für Bildung und Forschung (03DU0GO3-3) and the Deutsche Forschungsgemeinschaft (Heisenberg fellowship S. Siegesmund) for financial support of the recent research project. Furthermore, we would like to thank F. J. Brosch (University of Graz, Austria) and T. Popp (University of Kiel, Germany) for their constructive and helpful reviews. We are grateful to P. Machner and B. Middendorf (both from the University of Kassel) for their aid in performing the abrasive strength measurements. Thanks go to Klaus Ullemeyer and Peter Spalthoff (both University of Goettingen) for their help concerning the analysis of texture data.

References

AZZONI, A., BAILO, F., RONDENA, E. & ZANINETTI, A. 1996. Assessment of texture coefficient for different rock types and correlation with uniaxial compressive strength and rock weathering. *Rock Mechanics and Rock Engineering*, **29**, 39–46.

BALSLEY, J. R. & BUDDINGTON, A. F. 1960. Magnetic susceptibility anisotropy and fabric of some Adirondack Granites and Orthogneisses. *American Journal of Science*, **258-A**, 6–20.

BORRADAILE, G. J. 1987. Anisotropy of magnetic susceptibility; rock composition versus strain. *Tectonophysics*, **138**, 327–329.

BORRADAILE, G. J. 1988. Magnetic susceptibility, petrofabrics and strain. *Tectonophysics*, **156**, 1–20.

BROSCH, F. J., SCHACHNER, K., BLUEMEL, M. & FASCHING, A. 2000. Preliminary investigation results on fabrics and related mechanical properties of an anisotropic gneiss. *Journal of Structural Geology*, **22**, 1773–1787.

CHRISTOFFERSEN, R. & KRONENBERG, A. K. 1993. Dislocation interactions in experimentally deformed biotite. *In*: STEPHEN, H. K., SYLVESTER, A. G., TULLIS, J., WENK, H. R. & TREAGUS, S. H. (eds) Microstructures and rheology of rocks and rock-forming minerals; a collection of papers in honor of John Christie's 60th birthday. *Journal of Structural Geology*, **15**(9–10), 1077–1095.

DEARMAN, W. R., BAYNES, F. J. & IRFAN, T. Y. 1978. Engineering grading of weathered granite. *Engineering Geology*, **12**, 345–374.

DIN 22024, 1989. *Rohstoffuntersuchungen im Steinkohlenbergbau: Bestimmung der Spaltzugfestigkeit von Festgesteinen*. Beuth Verlag, Berlin.

DIN 52108, 1988. *Pruefung anorganischer nichtmetallischer Werkstoffe; Verschleißpruefung mit der Schleifscheibe nach Boehme*. Beuth Verlag, Berlin.

DIN EN 1341, 2000. *Platten aus Naturstein fuer Aussenbereiche: Anforderungen und Pruefverfahren*. Beuth Verlag, Berlin.

DIN EN 1342, 2000. *Pflastersteine aus Naturstein fuer Aussenbereiche: Anforderungen und Pruefverfahren*. Beuth Verlag, Berlin.

DIN EN 1343, 2000. *Bordsteine aus Naturstein fuer Aussenbereiche: Anforderungen und Pruefverfahren*. Beuth Verlag, Berlin.

DIN EN 1926, 1999. *Pruefverfahren fuer Naturstein: Bestimmung der Druckfestigkeit*. Beuth Verlag, Berlin.

DUERRAST, H., SIEGESMUND, S. & PRASAD, M. 1999. Die Schadensanalyse von Naturwerksteinen mittels Ultraschalldiagnostik: Moeglichkeiten und Grenzen. *Zeitschrift der deutschen Geologischen Gesellschaft*, **150**, 359–374.

DUEVEL, B. & HAIMSON, B. 1997. Mechanical characterization of pink Lac du Bonnet Granite; evidence of nonlinearity and anisotropy. *In*: KIM, K. (eds) ISRM international symposium, NY Rocks '97. *International Journal of Rock Mechanics and Mining Sciences and Geomechanics Abstracts*, **34**, 543.

ERSOY, A. & WALLER, M. D. 1995. Textural characterisation of rocks. *Engineering Geology*, **39**, 123–136.

GOTTSCHALK, R. R., KRONENBERG, A. K., RUSSELL, J. E. & HANDIN, J. 1990. Mechanical anisotropy of gneiss; failure criterion and textural sources of directional behavior. *Journal of Geophysical Research, B, Solid Earth and Planets*, **95**, 21,613–21,634.

HANDY, M. R. 1990. The solid-state flow of polymineralic rocks. *Journal of Geophysical Research, B, Solid Earth and Planets*, **95**, 8647–8661.

HOWARTH, D. F. & ROWLANDS, J. C. 1987. Quantitative assessment of rock texture and correlation with drillability and strength properties. *Rock Mechanics and Rock Engineering*, **20**, 57–85.

HROUDA, F. 1982. Magnetic anisotropy of rocks and its application in geology and geophysics. *Geophysical Surveys*, **5**, 37–82.

JELINEK, V. 1977. The statistical theory of measuring anisotropy of magnetic susceptibility of rocks and its application. *Geofyzika Brno*, **1**, 1–88.

JELINEK, V. 1981. Characterization of the magnetic fabric of rocks. *Tectonophysics*, **79**, T63–T67.

JORDAN, P. 1988. The rheology of polymineralic rocks; an approach. *In*: ZANKL, H., BELLIERE J., & PRASHNOWSKY, A. (eds) Detachment and shear. *Geologische Rundschau*, **77**(1), 285–294.

JUCKENACK, C. 1990. *Beitrag der Anisotropie der magnetischen Suszeptibilitaet (AMS) fuer Struktur- und Gefuegeuntersuchungen von Metamorphiten: Einzelbeispiele und regionale Anwendung im Spessart-Kristallin*. PhD Thesis, Georg- August-Universitaet Goettingen, Germany.

KOCH, A. & SIEGESMUND, S. 2002. Bowing of marble panels: on-site damage analysis from the Oeconomicum building at Goettingen (Germany). *In*: SIEGESMUND, S., WEISS, T. & VOLLBRECHT, A. (eds) *Natural Stone, Weathering Phenomena, Conservation Strategies and Case Studies*. Geological Society, London, Special Publications, **205**, 299–314.

KORONEOS, E. G., TASSOJANNOPOULOS, A. I. & DIAMANTOPOULOU, A. 1980. On the mechanical and physical properties of ten Hellenic marbles. *Engineering Geology*, **16**, 263–290.

KRANZ, R. L. 1983. Microcracks in rocks; a review. *In*: FRIEDMAN, M. & TOKSOEZ, M. N. (eds) Continental tectonics; structure, kinematics and dynamics. *Tectonophysics*, **100**(1–3), 449–480.

KRONENBERG, A. K., KIRBY, S. H. & PINKSTON, J. 1990. Basal slip and mechanical anisotropy of biotite. *Journal of Geophysical Research, B, Solid Earth and Planets*, **95**, 19,257–19,278.

LEISS, B. & ULLEMEYER, K. 1999. Texture characterisation of carbonate rocks and some implications for the modeling of physical anisotropies, derived from idealized texture types. *Zeitschrift der Deutschen Geologischen Gesellschaft*, **150**(2), 259–274.

LI, C., PRIKRYL, R. & NORDLUND, E. 1998. The stress-strain behaviour of rock material related to fracture under compression. *In*: PUSCH, R. (ed.) Computational methods in engineering geology. *Engineering Geology*, **49**(3–4), 293–302.

MARES, V. M. & KRONENBERG, A. K. 1993. Experimental deformation of muscovite. *In*: STEPHEN, H. K., SYLVESTER, A. G., TULLIS, J., WENK, H. R. & TREAGUS, S. H. (eds) Microstructures and rheology of rocks and rock-forming minerals; a collection of papers in honor of John Christie's 60th birthday. *Journal of Structural Geology*, **15**(9–10), 1061–1075.

MEGLIS, I. L., GREENFIELD, R. J., ENGELDER, T. & GRAHAM, E. K. 1996. Pressure dependence of velocity and attenuation and its relationship to crack closure in crystalline rocks. *Journal of Geophysical Research, B, Solid Earth and Planets*, **101**, 17,523–17,533.

MUEGGE, D. 1898. Uebér Translationen und verwandte Erscheinungen in Krystallen. *Neues Jahrbuch Mineral. Geol. Paleontol.*, **1**, 71–158.

NAGARAJ, T. S. 1993. *Principles of Testing Soils, Rocks and Concrete*. Elsevier, Amsterdam.

NAGATA, T. 1961. *Rock Magnetism*. Maruzen, Tokyo.

PASSCHIER, C. W. & TROUW, R. A. J. 1996. *Microtectonics*. Springer, Berlin.

PECK, L., BARTON, C. C. & GORDON, R. B. 1985. Microstructure and the resistance of rock to tensile fracture. *Journal of Geophysical Research. B*, **90**, 11,533–11,546.

RASOLOFOSAON, P. N. J., RABBEL, W., SIEGESMUND, S. & VOLLBRECHT, A. 2000. Characterization of crack distribution; fabric analysis versus ultrasonic inversion. *Geophysical Journal International*, **141**, 413–434.

SCHILD, M., SIEGESMUND, S., VOLLBRECHT, A. & MAZUREK, M. 2001. Characterization of granite matrix porosity and pore-space geometry by in situ and laboratory methods. *Geophysical Journal International*, **146**, 111–125.

SCHULTZ, R. A. 1995. Limits on strength and deformation properties of jointed basaltic rock masses. *Rock Mechanics and Rock Engineering*, **28**, 1–15.

SEGALL, P. & POLLARD, D. D. 1980. Mechanics of discontinuous faults. *Journal of Geophysical Research*, **85**, 4337–4350.

SHEA, W. T. & KRONENBERG, A. K. 1992. Rheology and deformation mechanisms of an isotropic mica schist. *Journal of Geophysical Research, B, Solid Earth and Planets*, **97**, 15,201–15,237.

SHEA, W. T. & KRONENBERG, A. K. 1993. Strength and anisotropy of foliated rocks with varied mica contents. *In*: STEPHEN, H. K., SYLVESTER, A. G., TULLIS, J., WENK, H. R. & TREAGUS, S. H. (eds) Microstructures and rheology of rocks and rock-forming minerals; a collection of papers in honor of John Christie's 60th birthday. *Journal of Structural Geology*, **15**(9–10), 1097–1121.

SHELTON, G. L. 1981. *Experimental deformation of single and polyphase crustal rocks at high temperatures and pressures*. PhD Thesis, Brown University.

SIEGESMUND, S. 1996. The significance of rock fabrics for the geological interpretation of geophysical anisotropies. *Geotektonische Forschungen*, **85**, 1–123.

SIEGESMUND, S., VOLLBRECHT, A. & PROS, Z. 1993. Fabric changes and their influence on P-wave velocity patterns; examples from a polyphase deformed orthogneiss. *Tectonophysics*, **225**, 477–492.

SIEGESMUND, S., ULLEMEYER, K. & DAHMS, M. 1995. Control of magnetic rock fabrics by mica preferred orientation; a quantitative approach. *Journal of Structural Geology*, **17**, 1601–1613.

STACEY, F. D., LOVERING, J. F. & PARRY, L. G. 1961. Thermomagnetic properties, natural magnetic moments and magnetic anisotropy of some chondritic meteorites. *Journal of Geophysical Research*, **66**, 1523–1534

STAVROGIN, A. N., TARASOV, B. G. 2001. *Experimental Physics and Rock Mechanics: Results of Laboratory Studies*. Balkema, Lisse.

TECHMER, K. S. 1996. Element mobilization in a ductile shear zone from the Sesia-Lanzo zone (northern Italy): a microstructural, petrographical and chemical study. *Zeitschrift für geologische Wissenschaften*, **24**(5/6), 699–713.

TULLIS, T. E., HOROWITZ, F. G. & TULLIS, J. 1991. Flow laws of polyphase aggregates from end-member flow laws. *Journal of Geophysical Research, B, Solid Earth and Planets*, **96**, 8081–8096.

VOLLBRECHT, A., DUERRAST, H., KRAUS, J. & WEBER, K. 1994. Paleostress directions deduced from microcrack fabrics in KTB core samples and granites from the surrounding area. *Scientific Drilling*, **4**(5–6), 233–241.

VOLLBRECHT, A., STIPP, M. & OLESEN, N. O. 1999. Crystallographic orientation of microcracks in quartz and inferred deformation processes; a study on gneisses from the German Continental Deep Drilling Project (KTB). *In*: SCHMID STEFAN, M., HEILBRONNER, R. & STUENITZ, H. (eds) Deformation mechanisms in nature and experiment. *Tectonophysics*, **303**(1–4), 279–297.

WINKLER, E. M. 1994. *Stone in Architecture: Properties and Durability*. Springer-Verlag, Berlin.